RSC Advances

PAPER

View Article Online
View Journal | View Issue

Cite this: *RSC Adv.*, 2017, **7**, 1016

Synthesis of di(ethylene glycol)-functionalized diketopyrrolopyrrole derivative-based side chain-conjugated polymers for bulk heterojunction solar cells†

Rong-Ho Lee,*[a] Lun-Cheng Yang,[a] Jeng-Yue Wu[a] and Ru-Jong Jeng[b]

Received 3rd November 2016
Accepted 18th November 2016

DOI: 10.1039/c6ra26245g

www.rsc.org/advances

Polythiophenes (PTs) featuring di(ethylene glycol)-substituted 2,5-thienyl diketopyrrolopyrrole (DG-TDPP) moieties as conjugated units in the polymer backbone and *tert*-butyl-substituted triphenylamine (*t*TPA)-containing moieties as pendant units have been synthesized through Stille coupling. Incorporating the electron-deficient DG-TDPP moieties within the polymer backbone and appending the *t*TPA units promoted charge balance and efficient conjugation within the extended conjugated frameworks of the polymers, resulting in lower band gap energies and red-shifting the maximum UV-Vis absorption wavelength. The influence of the DG-TDPP content on the optical, electrochemical, and photovoltaic (PV) properties of the polymers has been studied. Incorporating a suitable content of DG-TDPP moieties in the polymer backbone enhanced the solar absorption ability and conjugation length of the PTs. The PV properties of bulk-heterojunction solar cells based on PT/fullerene derivatives improved after incorporating DG-TDPP units in the backbones of the side chain-conjugated PTs.

1. Introduction

Optoelectronic devices fabricated from conjugated polymers have attracted much attention recently because they can be processed simply and inexpensively over large areas with flexible shapes and light weight.[1–3] In the case of polymer solar cells (PSCs), major advances in solar energy conversion efficiencies have been accomplished by replacing the double-layer cell with a bulk-heterojunction (BHJ) blend for the photoactive layer.[4–6] For most BHJ cells, the photoactive layer is based on a blend of an electron-donor polymer and an electron-acceptor fullerene derivative, either [6,6]-phenyl-C_{61}-butyric acid methyl ester ($PC_{61}BM$) or [6,6]-phenyl-C_{71}-butyric acid methyl ester ($PC_{71}BM$).[7] An electron-donor polymer having a low band gap is crucial when attempting to harvest large amounts of solar radiation. Using this approach, PSCs have been obtained with high short-circuit current densities (J_{SC}).[8,9] Moreover, high charge mobility is also required of the polymer in PSCs to minimize charge recombination in the photoactive layer, and to achieve high degrees of charge collection and large values of J_{SC}.[10] In addition, the energy level of the lowest unoccupied molecular orbital (LUMO) of the polymer must be appropriately offset from that of the electron-acceptor fullerene derivative.[11] A polymer having a deep highest occupied molecular orbital (HOMO) energy level favors a PSC having a large open-circuit voltage (V_{OC}).[12,13] On the other hand, a phase-separated interpenetrating network featuring sizable fullerene derivative-based domains in the photoactive layer facilitates the efficient formation of free carriers, thereby providing PSCs displaying optimal photovoltaic (PV) properties.[14–16]

PSCs providing good PV performance have been studied widely in which the conjugated polymers contain p-type electron-donating groups and electron-donating and -withdrawing donor–acceptor (D–A)-type structures.[10,12,17] The bipolar characteristics of conjugated polymers containing electron- and hole-transporting moieties are responsible for the lower-energy band gaps and higher charge mobilities of the photoactive layers that can enhance the PV efficiencies of PSCs. In addition, polythiophene (PT) derivatives bearing electron-donating and -withdrawing pendant groups, so-called two-dimensional low band gap conjugated polymers, have been proposed by several groups for PSC applications.[18–26] PT derivatives bearing conjugated pendant units absorb broadly in the UV and visible regions and can, therefore, harvest greater amounts of solar light. Moreover, the pendant conjugated moieties can enhance the charge mobilities of the polymers. Recently, we synthesized a series of PTs presenting pendant conjugated triphenylamine (TPA)- or carbazole-containing moieties as side chains.[27] Although the TPA- or carbazole-based conjugated pendant

[a]*Department of Chemical Engineering, National Chung Hsing University, Taichung 402, Taiwan. E-mail: rhl@dragon.nchu.edu.tw; Fax: +886-4-22854734; Tel: +886-4-22854308*

[b]*Institute of Polymer Science and Engineering, National Taiwan University, Taipei 106, Taiwan*

† Electronic supplementary information (ESI) available. See DOI: 10.1039/c6ra26245g

moieties enhanced the conjugation of the PTs, the cutoff wavelength of the absorption of these p-type conjugated polymers remained less than 750 nm. In addition, electron-deficient moieties, including benzothiadiazole and 2,5-thienyl diketopyrrolopyrrole (TDPP) units, have been incorporated into the backbones of polymers presenting electron-donating conjugated pendant units.[28–32] The presence of TDPP units in the polymer backbone enhanced the absorption edge to wavelengths of up to 1000 nm.[33–35] Unfortunately, increasing the TDPP content decreased the solubility of the polymers, due to increased degrees of π–π stacking among the polymer chains. The power conversion efficiencies (PCEs) of such polymer-based PSCs are not high.[33,34] Therefore, precise control over the molar ratio of electron-donating and -withdrawing units in a polymer chain is necessary to optimize the solubility and the optical and PV performance of their devices.

To validate these ideas, we synthesized a series of PTs (**PEGA11**, **PEGA12**, **PEGA13**) featuring di(ethylene glycol)-substituted 2,5-thienyl diketopyrrolopyrrole (DG-TDPP) moieties as conjugated units in the polymer backbones and *tert*-butyl-substituted triphenylamine (*t*TPA)-containing moieties as pendant units. We expected the conjugated DG-TDPP units with di(ethylene glycol) segments as flexible chains would improve the solubility of the PTs. We used UV-Vis absorption spectroscopy and cyclic voltammetry (CV) to study the effect of the DG-TDPP content on the photophysical and electrochemical properties of the polymers. We also employed atomic force microscopy (AFM) and transmission electron microscopy (TEM) to study the morphologies of thin films prepared from PT/$PC_{61}BM$ blends. We then fabricated PSCs having the conventional structure indium tin oxide (ITO)-coated glass/hole-transporting medium (HTM)/photoactive layer/LiF (0.5 nm)/Al (100 nm), by spin-coating a blend of each PT with $PC_{61}BM$ (or $PC_{71}BM$) to form a composite film-type photoactive layer on the HTM layer deposited on the ITO-coated glass. Based on the evaluated PV performance of these PSCs, we determined the influence of the DG-TDPP content of our PTs.

2. Experimental details

2.1 Chemicals

Potassium carbonate (K_2CO_3) *N*-bromosuccinimide (NBS), tris(dibenzylideneacetone)dipalladium(0) [$Pd_2(dba)_3$], tri(*o*-tolyl)phosphine [P(*o*-tolyl)$_3$], 2-(2-ethoxyethoxy)ethyl bromide, and other reagents and chemicals were purchased from Aldrich, Alfa, Acros, and TCI Chemical, and used as received. Chloroform ($CHCl_3$), dimethylformamide (DMF), toluene, and *o*-dichlorobenzene (*o*-DCB) were freshly distilled over appropriate drying agents, then purged with N_2, prior to use. 3,6-Di(thien-2-yl)-2,5-dihydropyrrolo[3,4-*c*]pyrrole-1,4-dione (**1**), 2,5-bis(-trimethylstannyl)thiophene (**4**), and (*E*)-4-(5-(2-(2,5-dibromothiophen-3-yl)vinyl)thien-2-yl)-*N*,*N*-((4,40-di-*tert*-butyl)diphenyl) aniline (**5**) were synthesized according to the literature.[27,35,36] The syntheses of 3,6-di(thien-2-yl)-2,5-di(2-(2-ethoxyethoxy) ethyl)-pyrrolo[3,4-*c*]pyrrole-1,4-dione (**2**) and 3,6-di(5-bromothien-2-yl)-2,5-di(2-(2-ethoxyethoxy)ethyl)pyrrolo[3,4-*c*]pyrrole-1,4-dione (**3**) are illustrated in Scheme 1. The syntheses of PTs (**PEGA11**, **PEGA12**, and **PEGA13**) featuring DG-TDPP moieties as conjugated units in the polymer backbones and *t*TPA-containing moieties as side chains are also illustrated in Scheme 1.

2.2 Synthesis

3,6-Di(thien-2-yl)-2,5-di(2-(2-ethoxyethoxy)ethyl)pyrrolo[3,4-*c*]pyrrole-1,4-dione (2). A solution of compound **1** (2.50 g, 8.33 mmol), K_2CO_3 (3.83 g, 27.80 mmol), and [18]-crown-6 (0.250 g, 0.95 mmol) in dry DMF (50 mL) was stirred at 120 °C under N_2 for 10 min and then a solution of 2-(2-ethoxyethoxy)ethyl bromide (4.17 mL, 27.5 mmol) in dry DMF (30 mL) was added dropwise. The resulting solution was heated with stirring for 20 h. After cooling to room temperature, the mixture was partitioned between CH_2Cl_2 and water; the organic phase was dried ($MgSO_4$), filtered, and evaporated to dryness. The residue was purified chromatographically (SiO_2; EtOAc/hexane, 1 : 4) to provide a dark-red solid (1.82 g, 41.9%). ^{1}H NMR (δ/ppm, 600 MHz, $CDCl_3$): 1.15 (t, 6H), 3.44 (q, 4H), 3.52 (t, 4H), 3.62 (t, 4H), 3.79 (t, 4H), 4.27 (t, 4H), 7.25 (t, 2H), 7.63 (d, 2H), 8.73 (d, 2H). Anal. calcd for $C_{26}H_{32}N_2O_6S_2$: C, 58.67; H, 6.02; N, 5.26; O, 18.05; S, 12.0. Found: C, 58.65; H, 6.07; N, 5.24; O, 18.04; S, 11.97.

3,6-Di(5-bromothien-2-yl)-2,5-di(2-(2-ethoxyethoxy)ethyl)pyrrolo[3,4-*c*]pyrrole-1,4-dione (3). A solution of **4** (0.53 g, 1.0 mmol) in $CHCl_3$ (30 mL) was stirred at room temperature for 10 min and then a solution of NBS (0.45 g, 2.3 mmol) in $CHCl_3$ (30 mL) was added dropwise. The resulting solution was stirred at room temperature for 12 h. The mixture was then partitioned between CH_2Cl_2 and water; the organic phase was dried ($MgSO_4$), filtered, and evaporated to dryness. The residue was recrystallized in MeOH to provide a purple solid (0.29 g, 42.0%). ^{1}H NMR (δ/ppm, 600 MHz, $CDCl_3$): 1.16 (t, 6H), 3.45 (q, 4H), 3.51 (t, 4H), 3.62 (t, 4H), 3.78 (t, 4H), 4.17 (t, 4H), 7.20 (d, 2H), 8.48 (d, 2H). Anal. calcd for $C_{26}H_{30}N_2O_6S_2Br_2$: C, 45.22; H, 4.35; N, 4.06; O, 13.91; S, 9.28. Found: C, 45.28; H, 4.31; N, 4.03; O, 13.86; S, 9.31.

PEGA11. A solution of **5** (0.35 g, 0.50 mmol), **6** (0.41 g, 1.0 mmol), and **7** (0.35 g, 0.50 mmol) in dry toluene (30 mL) was stirred at room temperature under N_2 for 10 min and then a solution of $Pd_2(dba)_3$ (36.6 mg, 0.04 mmol) and P(*o*-tolyl)$_3$ (48.7 mg, 0.16 mmol) in dry toluene (10 mL) was added dropwise. The resulting solution was heated with stirring at 90 °C for 48 h. After cooling to room temperature, the solution was poured into MeOH (100 mL). The precipitate was filtered off, placed in a Soxhlet thimble, and extracted sequentially with MeOH, hexane, acetone, $CHCl_3$, and *o*-DCB. The polymer **PEGA11** was recovered from the *o*-DCB fraction through rotary evaporation. Drying under vacuum for 24 h provided a black solid (0.24 g, 21.4%). ^{1}H NMR (δ/ppm, 600 MHz, CD_2Cl_2): 0.75–1.39 (m, 28H), 3.15–3.71 (m, 20H), 6.35–7.62 (m, 28H). Anal. calcd for $[(C_{26}H_{30}N_2O_6S_2)(C_{40}H_{37}NS_3)_{1.25}]$: C, 69.42; H, 5.80; N, 3.46; O, 7.31; S, 14.01. Found: C, 69.55; H, 5.75; N, 3.53; O, 7.37; S, 13.80.

PEGA12. Using the procedure described above for the synthesis of **PEGA11**, the reaction of **5** (0.23 g, 0.33 mmol), **6** (0.41 g, 1.0 mmol), and **7** (0.47 g, 0.67 mmol) provided **PEGA12**

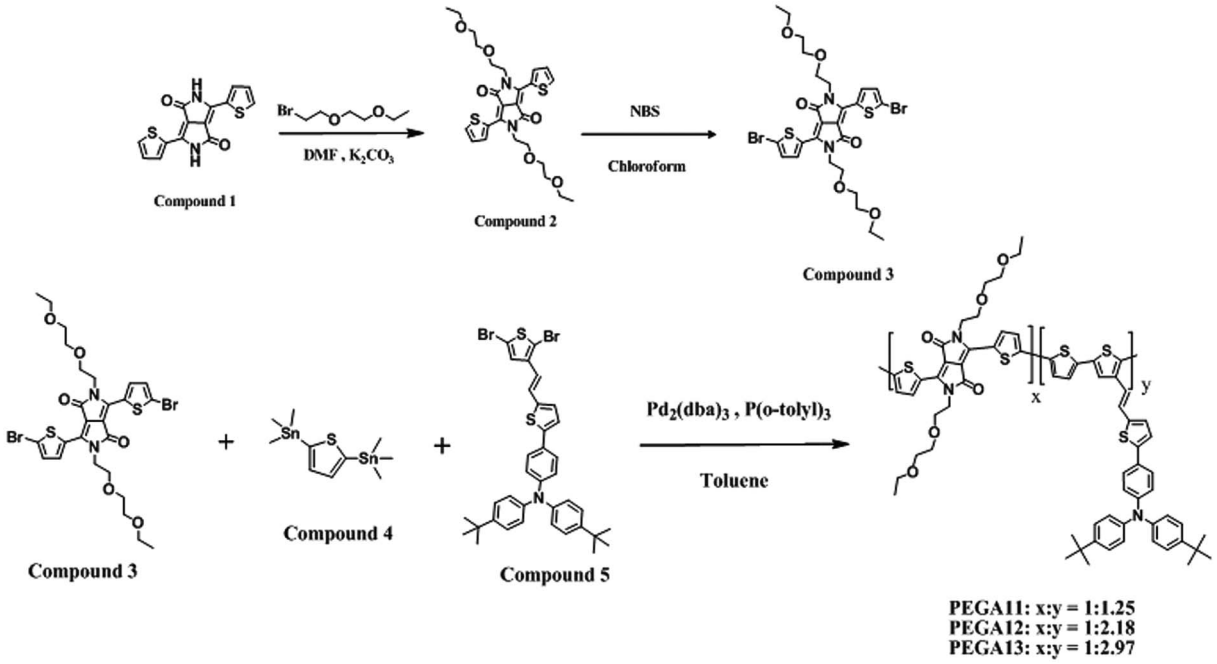

Scheme 1 Synthesis of compounds **2**, **3**, **PEGA11**, **PEGA12**, and **PEGA13**.

as a black solid (0.16 g, 14.4%). ^{1}H NMR (δ/ppm, 600 MHz, CD_2Cl_2): 0.75–1.40 (m, 45H), 3.10–3.75 (m, 20H), 6.30–7.60 (m, 46H). Anal. calcd for $[(C_{26}H_{30}N_2O_6S_2)(C_{40}H_{37}NS_3)_{2.18}]$: C, 71.61; H, 5.83; N, 3.09; O, 5.06; S, 14.41. Found: C, 71.59; H, 5.89; N, 3.05; O, 5.10; S, 14.37.

PEGA13. Using the procedure described above for the synthesis of **PEGA11**, the reaction of **5** (0.17 g, 0.25 mmol), **6** (0.41 g, 1.0 mmol), and **7** (0.53 g, 0.75 mmol) provided **PEGA13** as a black solid (0.26 g, 23.4%). ^{1}H NMR (δ/ppm, 600 MHz, CD_2Cl_2): 0.65–1.40 (m, 60H), 3.05–3.75 (m, 20H), 6.30–7.42 (m, 60H). Anal. calcd for $[(C_{26}H_{30}N_2O_6S_2)(C_{40}H_{37}NS_3)_{2.97}]$: C, 72.64; H, 5.85; N, 2.90; O, 4.01; S, 14.64. Found: C, 72.60; H, 5.91; N, 2.88; O, 4.10; S, 14.51.

2.3 Characterization of copolymers

^{1}H NMR (600 MHz) spectra were recorded using a Varian Unity Inova spectrometer. The average molecular weights of the polymers were measured by means of gel permeation chromatography (GPC), using a Waters chromatography system (717 plus Autosampler) equipped with two Waters Styragel linear columns, employing polystyrene (PS) standards and THF as the eluent. The glass transition temperatures (T_g) and thermal decomposition temperatures (T_d; temperatures at which weight loss reached 5%) of the copolymers were determined through differential scanning calorimetry (TA Instruments, DSC-2010) and thermogravimetric analysis (TA Instruments, TGA-2050), respectively. Both analyses were performed under a N_2 atmosphere at scanning (both heating and cooling) rates of 10 °C min^{-1}. The temperatures at the intercepts of the curves in the thermograms (endothermic, exothermic, or weight loss) with the leading baseline were taken as estimates of the values of T_g and T_d. Absorption spectra were recorded using a Hitachi U3010 UV-Vis spectrometer; dilute *o*-DCB solutions of the PTs were filtered through a 0.45 μm filter to remove insoluble materials prior to spectral measurement. The redox potentials of the polymers were determined using a CHI 611D electrochemical analyzer (scanning rate: 50 mV s^{-1}) equipped with Pt electrodes and an Ag/Ag$^+$ (0.10 M $AgNO_3$ in MeCN) reference electrode in an anhydrous, N_2-saturated solution of 0.1 M Bu_4NClO_4 in MeCN. Bu_4NClO_4 (98%, TCI) was recrystallized three times from MeOH and water (1 : 1) and then dried at 100 °C under reduced pressure. A Pt plate coated with a thin polymer film was used as the working electrode; a Pt wire and an Ag/Ag$^+$ electrode were used as the counter and reference electrodes, respectively. The electrochemical potential was calibrated against ferrocene/ferrocenium. The morphologies of films prepared from PT/$PC_{61}BM$ blends were studied using an atomic force microscope (AFM, Seiko SII SPA400) operated in the tapping mode and a transmission electron microscope (TEM, JEOL JEM-1400).

2.4 Fabrication and characterization of PSCs

The PSCs fabricated in this study had the structure ITO-coated glass/HTM/photoactive layer/LiF (0.5 nm)/Al (100 nm), where the photoactive layer comprised an interpenetrating network of a PT and a fullerene derivative ($PC_{61}BM$ or $PC_{71}BM$). ITO-coated glass (sheet resistance: 20 Ω per square) was purchased from Applied Film Corp. $PC_{61}BM$ and $PC_{71}BM$ were purchased from Nanocarbon Corp. and used as received. The PSCs were fabricated as follows: glass substrates with patterned ITO electrodes were washed well and then cleaned through O_2 plasma treatment. A thin film of the HTM, poly(3,4-ethylenedioxythiophene) doped with poly(styrene sulfonate) (PEDOT:PSS, AI4083, Heraeus Clevios GmbH), was deposited on the ITO layer through spin-casting. The sample was dried at 150 °C for 30 min in

a glove box. A solution of a mixture of PT and $PC_{61}BM$ (or $PC_{71}BM$) (30 mg mL^{-1} in *o*-DCB) was stirred overnight, then filtered through a 0.2 μm polytetrafluoroethylene (PTFE) filter and spin-coated (1500 rpm, 30 s) onto the HTM layer to prepare the PT/$PC_{61}BM$ (or $PC_{71}BM$) composite film-based photoactive layer. The sample was dried at 110 °C for 10 min in a glove box. In a high-vacuum chamber, the Ca/Al-based cathode was thermally deposited onto the PT/$PC_{61}BM$ (or $PC_{71}BM$) composite layer. The active area of the PSC was 0.04 cm^2. After electrode deposition, the PSC was encapsulated. The cathode deposition rate was determined using a quartz thickness monitor (STM-100/MF, Sycon). The thicknesses of the thin films were determined using a surface texture analysis system (3030ST, Dektak). The PV properties of the PSCs were measured using a programmable electrometer equipped with current and voltage sources (Keithley 2400) under illumination with solar-simulating light (100 mW cm^{-2}) from an AM1.5 solar simulator (NewPort Oriel 96000).

3. Results and discussion

3.1 Characterization of PTs

The conjugated PTs were synthesized through Stille coupling of DG-TDPP (**3**), 2,5-bis(trimethylstannyl)thiophene (**4**), and *t*TPA-containing thiophene derivative (**5**). The chemical structures of the monomers were confirmed using ^{1}H NMR spectroscopy and elemental analysis. ^{1}H NMR spectra of compounds **3–5** and PTs are shown in Fig. S1 and S2,† respectively. Chemical shifts and relative intensities of the signals in the ^{1}H NMR spectra were in agreement with the proposed structures of compounds **3–5** and PTs. The repeat unit ratios (*x*/*y*; see Scheme 1) of the PTs (**PEGA11**, **PEGA12**, and **PEGA13**) were modulated by controlling the feed ratio of the DG-TDPP and conjugated pendant *t*TPA-containing thiophene derivative **5**. For the copolymers **PEGA11**, **PEGA12**, and **PEGA13**, the actual values of *x*/*y* were determined from the relative integral areas of their peaks at 6.20–7.60 ppm (representing protons of the vinylene, phenyl, and thiophene groups) and 3.10–3.80 [representing protons of di(ethylene glycol) groups] in the ^{1}H NMR spectra. The values of *x*/*y* of **PEGA11**, **PEGA12**, and **PEGA13** were approximately 1 : 1.25, 1 : 2.18, and 1 : 2.97, respectively. Using GPC with THF as the eluent and PS internal standards, we determined the number-average molecular weights (M_n) and weight-average molecular weights (M_w) of the conjugated PTs. As summarized in Table 1, the values of M_n and M_w of the conjugated polymers were in the ranges 6.5–13.5 and 14.5–28.4 kg mol^{-1}, respectively. The average molecular weights of **PEGA11** and **PEGA12** were much lower than that of **PEGA13**. The early termination of the propagation of the polymer chains resulted from poor solubility of the polymers in the reaction solution and, accordingly, their precipitation. As a result, we observed relatively lower average molecular weights for **PEGA11** and **PEGA12**. Relatively poorer solubility of **PEGA11** and **PEGA12** was due to their higher contents of DG-TDDP units. In fact, relatively poorer solubility of PT with higher DG-TDDP contents was attributed to the strong intermolecular hydrogen-bonding interactions between the lactam units.[37] Nevertheless, these three conjugated copolymers were all soluble in common organic solvents, including THF, CH_2Cl_2, $CHCl_3$, and *o*-DCB. Excellent solubility is favorable for the formation of the solution-processed PTs based photo-active layers.

Table 1 Average molecular weights and thermal properties of the PTs

PT	M_n (kg mol^{-1})	M_w (kg mol^{-1})	$T_g{}^a$ (°C)	$T_d{}^b$ (°C)
PEGA11	6.5	14.5	113.4	319.8
PEGA12	7.8	16.4	112.8	347.1
PEGA13	13.5	28.4	120.9	398.5

^{a} T_g: measured at a heating rate of 10 °C min^{-1}. ^{b} T_d: temperature at which weight loss reached 5%.

The operational stability of a PSCs is directly related to the thermal stability of its component conjugated polymer. Thus, high values of T_g and T_d are desirable. We measured the values of T_g and T_d of our conjugated copolymers by means of thermal analyses using DSC and TGA (Table 1). The values of T_d for **PEGA13**, **PEGA12**, and **PEGA11** were 398.5, 347.1, and 319.8 °C, respectively. The thermal stability of the PTs decreased upon increasing the DG-TDPP content. Moreover, we determined glass transition temperatures from the second round of DSC

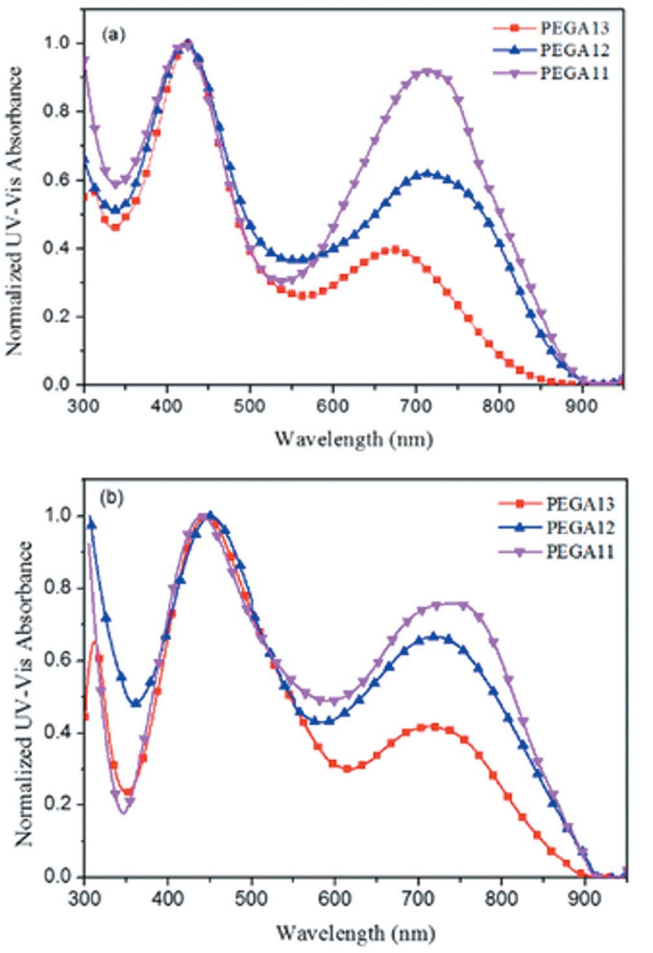

Fig. 1 Normalized UV-Vis absorption spectra of PTs (a) in *o*-DCB solution and (b) as thin films.

Table 2 Optical properties, electrochemical onset potentials, and electronic energy levels of the PTs

PT	$\lambda_{max}^{abs\ a}$ (nm)	$\lambda_{max}^{abs\ b}$ (nm)	E_g^{optc} (eV)	E_{on}^{ox} (V)	HOMO (eV)	LUMO (eV)
PEGA11	420, 717	445, 740	1.40	0.40	−5.11	−3.71
PEGA12	423, 715	450, 722	1.41	0.38	−5.09	−3.68
PEGA13	426, 673	447, 720	1.47	0.26	−4.97	−3.50

[a] Maximum absorption wavelength of polymer in solution. [b] Maximum absorption wavelength of polymer as thin film. [c] Calculated value of E_g from the onset absorption (λ_{onset}^{abs}) of polymer thin film: $E_g = 1240/\lambda_{onset}$.

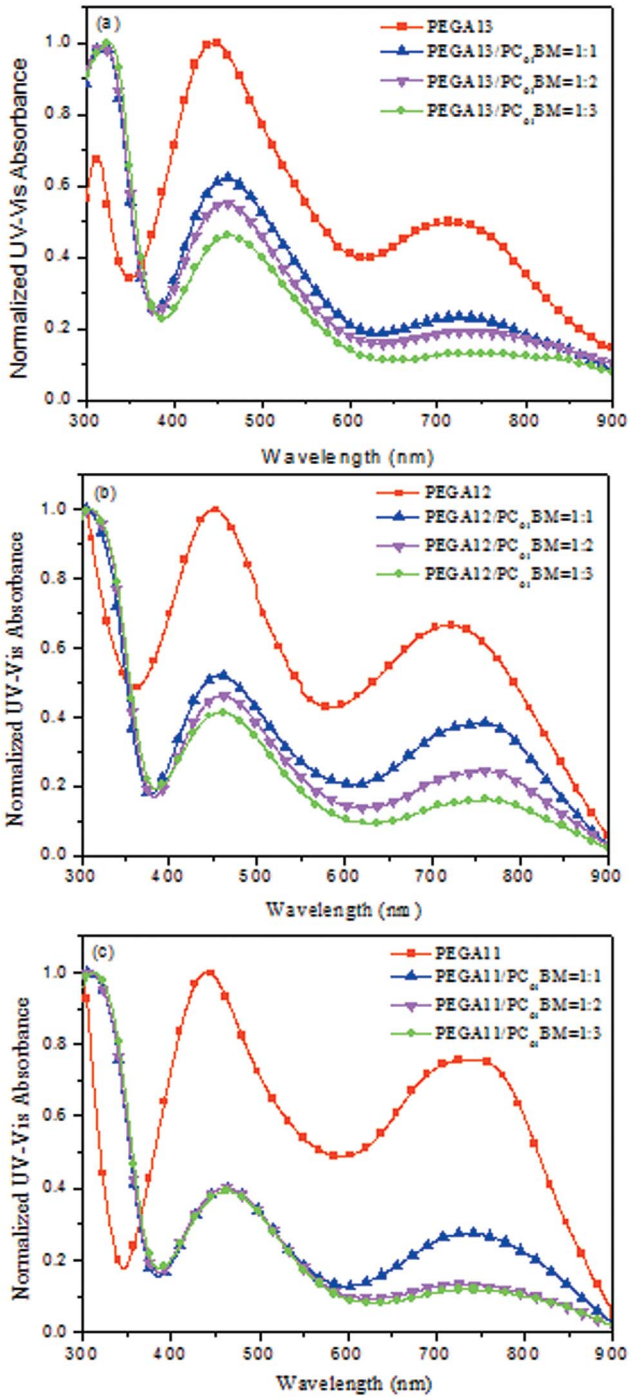

Fig. 2 Normalized UV-Vis absorption spectra of (a) **PEGA13**/$PC_{61}BM$, (b) **PEGA12**/$PC_{61}BM$, and (c) **PEGA11**/$PC_{61}BM$ blend films.

heating scans. The values of T_g for **PEGA13**, **PEGA12**, and **PEGA11** were 120.9, 112.8, and 113.4 °C, respectively, making them suitable for PSC applications. Relatively low values of T_g resulted from the polymers having higher contents of flexible di(ethylene glycol)-substituted diketopyrrolopyrrole units. In addition, we observed a single endothermic glass transition for each conjugated copolymer, implying that the diketopyrrolopyrrole conjugated units and electron-donating bulky *t*TPA-containing pendant moieties were distributed homogeneously.

3.2 Optical properties of PTs

Fig. 1 presents normalized UV-Vis absorption spectra of the DG-TDPP-containing PTs as solutions in *o*-DCB and as solid films. Table 2 summarizes their photophysical properties. The absorptions of the DG-TDPP-containing PTs in *o*-DCB ranged from 325 to 900 nm; each polymer displayed two broad absorption bands. We attribute the first absorption band, in the range 350–550 nm, to the n–π* transitions of the conjugated side chains and the π–π* transitions of the conjugated main chains. The second absorption band, in the range 550–900 nm, originated from intramolecular charge transfer (ICT) between the thiophene-based donor units and DG-TDPP-based acceptor units.[33,34] The absorption intensities of the second absorption band increased upon increasing the content of DG-TDPP units in the copolymers, both in solution and as thin films. Moreover, the red-shifts and full widths at half-maximum of the absorption bands of the copolymers in their film forms were greater

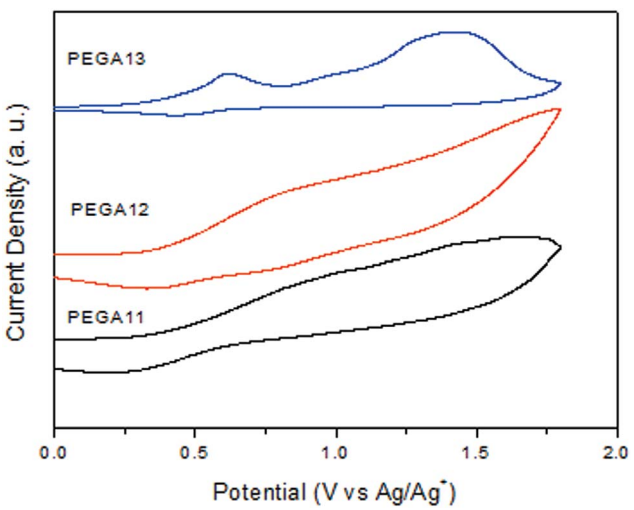

Fig. 3 Cyclic voltammograms of **PEGA11**, **PEGA12**, and **PEGA13**.

than those in solution, presumably because of strong non-covalent interactions (*e.g.*, π-stacking) between the polymer backbones and conjugated pendant units.[27,36]

We determined the band gap energies (E_g) of the conjugated polymers in their thin film states from the onset wavelengths of their absorption bands. Table 2 reveals that the values of E_g for **PEGA11**, **PEGA12**, and **PEGA13** were 1.40, 1.41, and 1.47 eV, respectively. The lower values of E_g were observed for the copolymers having higher contents of DG-TDPP units. In general, a broader absorption range and a lower band gap energy will improve the efficiency of solar light absorption of the photo-energy conversion layer in a PSC, resulting in the generation of a larger photocurrent.

Fig. 2 displays normalized UV-Vis absorption spectra of the PT/$PC_{61}BM$ composite films. The absorption bands of the DG-TDPP-containing copolymers ranged from 375 to 900 nm,

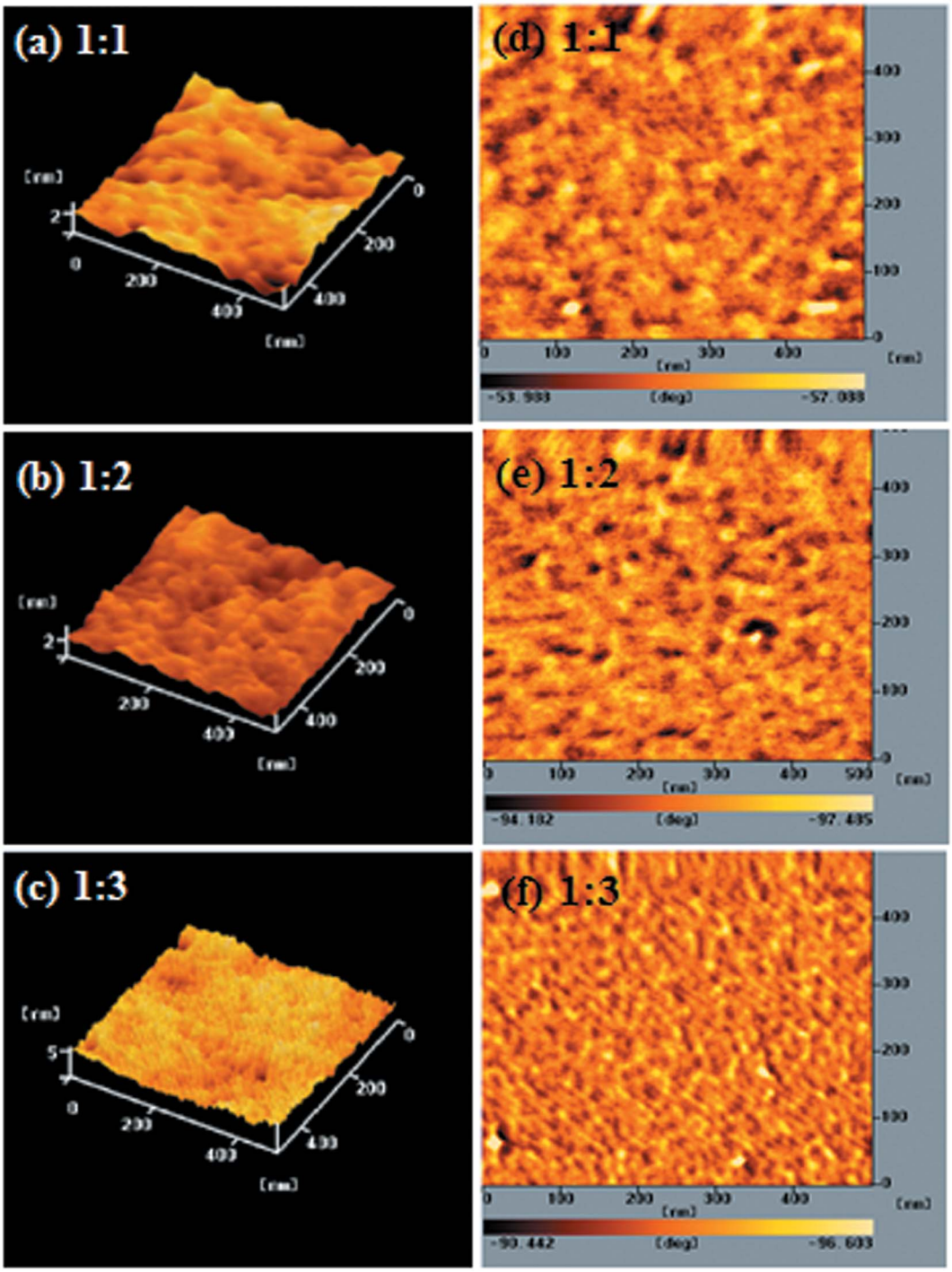

Fig. 4 AFM (tapping mode) (a–c) topographic and (d–f) phase images of **PEGA13**/$PC_{61}BM$ blend films [(a and d) 1 : 1, w/w; (b and e) 1 : 2, w/w; (c and f) 1 : 3, w/w] after annealing at 110 °C for 10 min.

while the absorption band of $PC_{61}BM$ ranges from 300 to 375 nm. The maximum absorption peaks of the conjugated copolymer and $PC_{61}BM$ appeared near 425 and 325 nm, respectively. Moreover, the absorption intensity of the conjugated polymer decreased as the $PC_{61}BM$ content increased for these PT/$PC_{61}BM$ composite films. From the viewpoint of photon absorption, employing less $PC_{61}BM$ in the photoactive layer would be preferred. Nevertheless, the typical stoichiometry of polymer/$PC_{61}BM$ blends, optimal for devices in several PSC systems, ranges from 1 : 1 to 1 : 4 by weight.[38] A high proportion of $PC_{61}BM$ limits the optical absorption in the composite layer because the absorption of $PC_{61}BM$ is quite inefficient in the visible region.

3.3 Electrochemical properties of PTs

Because the PV performance of a PSC is related to the electrochemical behavior of its conjugated polymer, we employed CV to investigate the electrochemical behavior of our PTs and estimate the energy levels of their HOMOs. Fig. 3 presents the oxidation behavior in the CV curves of the PTs. Table 2 summarizes the electrochemical properties of the copolymers. The oxidation potentials (E_{on}^{ox}) of **PEGA11**, **PEGA12**, and **PEGA13** were 0.40, 0.38, and 0.26 V, respectively. From those values, we calculated the HOMO energy levels of the copolymers according to the equation

$$\text{HOMO} = -e(E_{on}^{ox} - E_{on}^{ox}, \text{ferrocene} + 4.71)\ (\text{eV})$$

where 4.71 eV is the energy level of ferrocene below the vacuum level and the value of E_{on}^{ox} of ferrocene/ferrocene^{+} is 0.09 V in 0.1 M Bu_4NClO_4/MeCN. The HOMO energy levels obtained for **PEGA11**, **PEGA12**, and **PEGA13** were −5.11, −5.09, and −4.97 eV, respectively. Lower HOMO energy levels were observed for the PTs having lower contents of *t*TPA-containing conjugated pendant units, suggesting lower electron-donating abilities for these polymers.[39] In addition, because no reversible n-doping process was evident in the CV spectra, we estimated the LUMO energy levels from the HOMO energy levels and the values of E_g determined from the UV-Vis absorption spectra, using the equation

$$\text{LUMO} = \text{HOMO} + E_g\ (\text{eV})$$

The calculated LUMO energy levels were −3.71 eV for **PEGA11**, −3.68 eV for **PEGA12**, and −3.50 eV for **PEGA13**. Lower LUMO levels were obtained for the PTs having higher contents of electron-deficient (*i.e.*, DG-TDPP) units. Thus, the electrochemical properties of these PTs could be tuned by incorporating electron-accepting DG-TDPP units into the polymer backbone. In general, the HOMO energy level of a p-type conjugated polymer is an important parameter affecting the performance of BHJ-type cells. High open-circuit voltages (V_{OC}) are typically obtained for PSCs fabricated from conjugated polymers having low HOMO energy levels.[12]

3.4 Morphology of thin films of PT/$PC_{61}BM$ blends

The performance of a PSC is strongly dependent on the morphology of the film of its conjugated polymer/fullerene derivative composite. To avoid recombination of excitons, the P/N heterojunction phase must be controlled at the nanoscale level.[27,36] We used AFM microscopy to investigate the compatibility and morphology of our conjugated polymer/$PC_{61}BM$ composite films. Fig. 4 displays topographic and phase-contrast images of **PEGA13**/$PC_{61}BM$ composite films (1 : 1, 1 : 2, and 1 : 3, w/w) after annealing at 110 °C for 10 min; Fig. S3 and S4 (ESI†) present the corresponding the topographic and phase-contrast images of the **PEGA11**/$PC_{61}BM$ and **PEGA12**/$PC_{61}BM$ composite films (1 : 1, 1 : 2, and 1 : 3, w/w). The phase-contrast images indicated that the distribution of the $PC_{61}BM$ units in the polymers was uniform for the DG-TDPP-containing PT/$PC_{61}BM$ composite films. In each case, we observed a phase-separated interpenetrating network with sizable $PC_{61}BM$ domains. Some degree of phase separation is critical for efficient formation of free carriers to provide PSCs with optimal PV properties. Moreover, the sizes of the phase separation domains decreased upon increasing the $PC_{61}BM$ content. The nanoscale phase separation was more obvious for the PT/$PC_{61}BM$ composite film having the higher $PC_{61}BM$ content (1 : 3, w/w). Larger interface area will be obtained for PT/$PC_{61}BM$ composite films having larger $PC_{61}BM$ contents and smaller domain sizes.

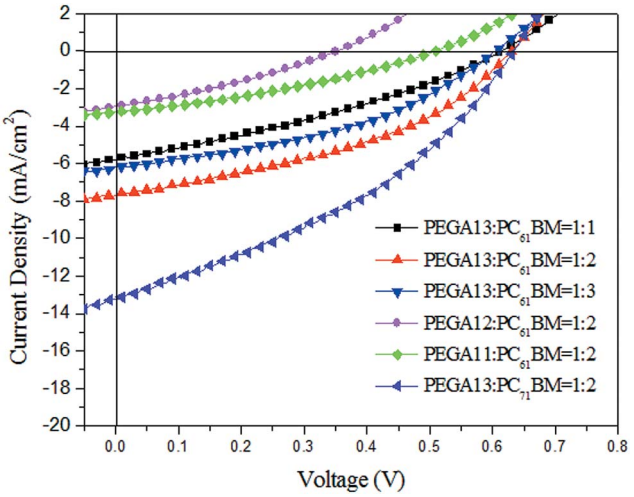

Fig. 5 Current density–potential characteristics of illuminated (AM 1.5G, 100 mW cm^{-2}) PSCs incorporating (**PEGA13**, **PEGA12**, **PEGA11**)/$PC_{61}BM$ and **PEGA13**/$PC_{71}BM$ blends.

3.5 PV properties of PSCs incorporating PT/$PC_{61}BM$ films

We used an optimized spin-coating procedure to fabricate PSCs incorporating PT/$PC_{61}BM$ blends as photoactive layers. Fig. 5 displays the photocurrent density–voltage plots of these PSCs; Table 3 summarizes the PV properties of these PSCs, including their values of V_{OC}, J_{SC}, fill factor (FF), and photoconversion efficiency (η). For the **PEGA13**/$PC_{61}BM$-based PSCs (PSC I-1–PSC I-3), the value of V_{OC} did not change significantly in response to the content of $PC_{61}BM$. Moreover, the values of J_{SC}, FF, and η of the PSCs increased upon increasing the $PC_{61}BM$ content. The

Table 3 Photovoltaic performance of PSCs incorporating films of (**PEGA13**, **PEGA12**, **PEGA11**)/$PC_{61}BM$ and **PEGA13**/$PC_{71}BM$ blends

PSC	Photoactive layer	PT/$PC_{61}BM$ (or $PC_{71}BM$) (w/w)	V_{OC} (V)	J_{SC} (mA cm^{-2})	FF	η (%)	Mobility (10^{-5} cm^2 V^{-1} s^{-1})
PSC I-1	**PEGA13**/$PC_{61}BM$	1 : 1	0.61	5.8	0.32	1.1	1.79
PSC I-2	**PEGA13**/$PC_{61}BM$	1 : 2	0.63	7.7	0.41	2.0	2.04
PSC I-3	**PEGA13**/$PC_{61}BM$	1 : 3	0.60	6.7	0.40	1.6	1.86
PSC II	**PEGA12**/$PC_{61}BM$	1 : 2	0.35	2.9	0.32	0.3	1.54
PSC III	**PEGA11**/$PC_{61}BM$	1 : 2	0.51	3.2	0.33	0.5	1.36
PSC IV	**PEGA13**/$PC_{71}BM$	1 : 2	0.67	9.0	0.42	2.5	3.17

highest values of J_{SC} and η were observed for the PSC based on a photoactive layer of **PEGA13**/$PC_{61}BM$ at a weight ratio of 1 : 2. Higher concentrations of $PC_{61}BM$ in the photoactive layer favored the formation of phase-separated interpenetrating networks with sizable domains, which in turn led to effective charge separation and charge transfer.[27] Typically, efficient dissociation of excitons and higher degrees of charge collection to the electrode are favorable for PSCs displaying enhanced values of J_{SC}. Nevertheless, an excessive content of $PC_{61}BM$ does not favor the charge transfer behavior and PV performance of PSCs. The PV performance of PSC I-3 was poorer than that of PSC I-2. This finding implies that the optimal PT-to-$PC_{61}BM$ composition was approximately 1 : 2 (w/w) for the **PEGA13**-based PSCs. In addition, the hole mobility of a photoactive layer also plays an important role affecting the PV performance of a PSC. We used the space-charge limited current method to measure the hole mobilities of our PT/$PC_{61}BM$ blend films, with a typical hole-only device structure of ITO/PEODT/PT:$PC_{61}BM$ (or $PC_{71}BM$)/Au.[40] Fig. 6 presents the results plotted as the current density (J) with respect to voltage (V). Table 3 summarizes the hole mobilities of the blend films. The hole mobility of the 1 : 2 (w/w) **PEGA13**/$PC_{61}BM$ blend film (2.04×10^{-5} cm^2 V^{-1} s^{-1}) was greater than those of the corresponding 1 : 1 (1.79×10^{-5} cm^2 V^{-1} s^{-1}) and 1 : 3 (1.86×10^{-5} cm^2 V^{-1} s^{-1}) blend films. The relatively higher hole mobility of the **PEGA13**/$PC_{61}BM$ (1 : 2, w/w) blend film resulted in the better PV performance of PSC I-2. On the other hand, the PV properties of the **PEGA11**- and **PEGA12**-based PSCs (PSC II and PSC III, respectively) were much poorer than those of the **PEGA13**-based PSCs, reflecting the lower average molecular weights and poorer hole mobilities of **PEGA11** and **PEGA12**. The hole mobilities of **PEGA11**/$PC_{61}BM$ and **PEGA12**/$PC_{61}BM$ were lower than that of **PEGA13**/$PC_{61}BM$ (Table 3).

To further improve the PV performance of the **PEGA13**-based PSCs, we introduced $PC_{71}BM$ as the electron-acceptor in the

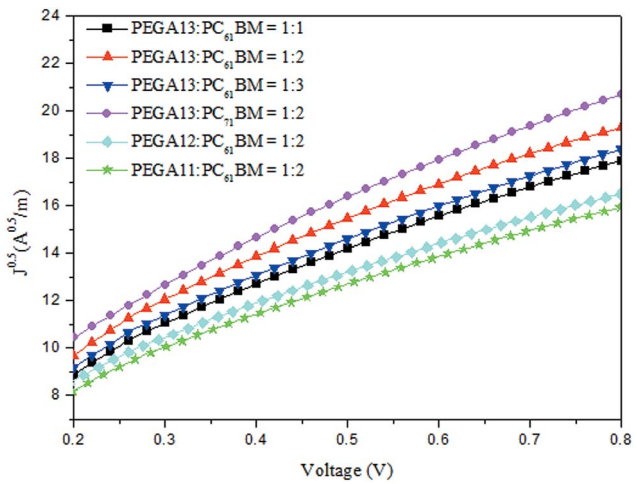

Fig. 6 Plots of $(J)^{0.5}$ *vs.* V of hole-only devices incorporating PT/$PC_{61}BM$ and **PEGA13**/$PC_{71}BM$ blends.

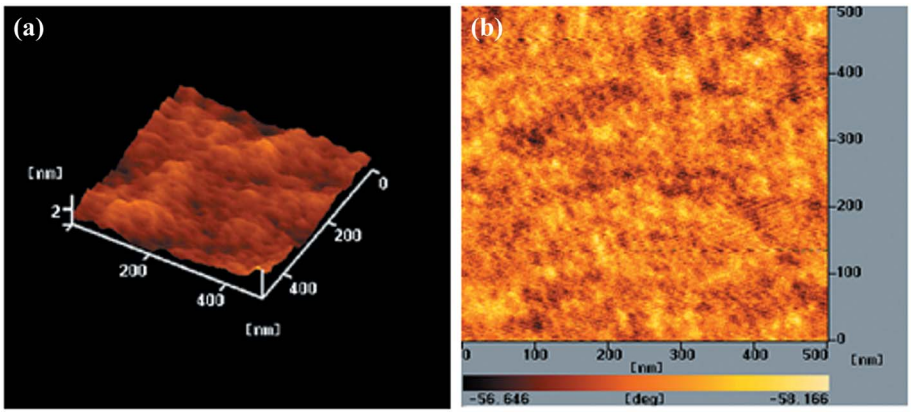

Fig. 7 AFM (tapping mode) (a) topographic and (b) phase images of the **PEGA13**/$PC_{71}BM$ (1 : 2, w/w) blend film after annealing at 110 °C for 10 min.

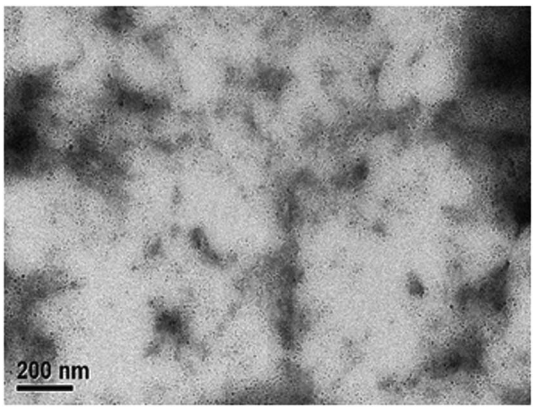

Fig. 8 TEM image of the **PEGA13**/$PC_{71}BM$ (1 : 2, w/w) blend film after annealing at 110 °C for 10 min.

photoactive layers of the PSCs. Fig. 5 displays the photocurrent density–voltage plots of the PSCs based on the **PEGA13**/$PC_{71}BM$ blend film (PSC IV). Table 3 summarizes the PV properties of these PSCs. Because the optimal composition of the **PEGA13**/$PC_{61}BM$ blend was 1 : 2 (w/w), we studied the PSC IV based on a **PEGA13**/$PC_{71}BM$ blend also having a composition of 1 : 2 (w/w). The AFM images in Fig. 7 indicate that phase-separated interpenetrating networks with sizable domains were formed in the photoactive layer for the **PEGA13**/$PC_{71}BM$ blend film. In addition, we used TEM to further characterize the distribution of $PC_{71}BM$ in the PT/$PC_{71}BM$ films. Fig. 8 presents the TEM image of the **PEGA13**/$PC_{71}BM$ blend film (1 : 2, w/w). The dark areas in the image represent $PC_{71}BM$ domains, because the electron scattering density of $PC_{71}BM$ is greater than that of the conjugated polymer. The formation of phase-separated interpenetrating networks with sizable domains in the photoactive layer was confirmed. The hole mobility of the 1 : 2 (w/w) **PEGA13**/$PC_{71}BM$ blend film was approximately 3.17×10^{-5} $cm^2\ V^{-1}\ s^{-1}$ (Table 3). As displayed in Fig. 5, we observed much higher values of J_{SC} and PCE for the PSCs based on the **PEGA13**/$PC_{71}BM$ blend films, as compared with those based on PT/$PC_{61}BM$ blends, presumably because of the stronger and broader absorption of $PC_{71}BM$ in the visible region and the greater hole mobility of the **PEGA13**/$PC_{71}BM$ blend film.[27] Apart from that, PV performance of the **PEGA13**/$PC_{71}BM$ based PSC was much better than that of the **r-TPATh-PT**/$PC_{71}BM$ based PSC.[24] As compared to the **r-TPATh-PT**, the incorporation of the electron-deficient DG-TDPP units onto the polymer backbone resulted in a broader absorption band for **PEGA13**. Therefore, better PV performance was observed for the **PEGA13** based PSC.

4. Conclusion

We have synthesized a series of PTs featuring di(ethylene glycol)-substituted 2,5-thienyl diketopyrrolopyrrole as conjugated units in the polymer backbones and *t*TPA-containing moieties as pendant units. Incorporating the electron-deficient DG-TDPP moieties into the polymer backbone and appending the *t*TPA units promoted charge balance and efficient conjugation within the extended conjugated frameworks of the polymers. The absorption ability and hole mobility of the PTs both improved upon optimization of the molar ratio of the *t*TPA-based electron-donating pendant units and the electron-withdrawing DG-TDPP units in the polymer chains. The PV performance of the **PEGA13**-based PSCs was better than those of the **PEGA12**- and **PEGA11**-based PSCs.

Acknowledgements

We thank the Ministry of Science and Technology (MOST) of Taiwan for financial support.

References

1 M. Helgesen, R. Sondergaard and F. C. Krebs, *J. Mater. Chem.*, 2010, **20**, 36.
2 J. D. Chen, C. Cui, Y. Q. Li, L. Zhou, Q. D. Ou, C. Li, Y. F. Li and J. X. Tang, *Adv. Mater.*, 2015, **27**, 1035.
3 Y. W. Su, W. H. Lin, Y. J. Hsu and K. H. Wei, *Small*, 2014, **10**, 4427.
4 Y. W. Su, S. C. Lan and K. H. Wei, *Mater. Today*, 2012, **15**, 554.
5 M. H. Chen, J. Hou, Z. Hong, G. Yang, S. Sista, L. M. Chen and Y. Yang, *Adv. Mater.*, 2009, **21**, 4238.
6 B. Xu, Z. Zheng, K. Zhao and J. Hou, *Adv. Mater.*, 2016, **28**, 434.
7 W. Yue, R. S. Ashraf, C. B. Nielsen, E. C. Fregoso, M. R. Niazi, S. A. Yousaf, M. Kirkus, H. Y. Chen, A. Amassian, J. R. Durrant and I. McCulloch, *Adv. Mater.*, 2015, **27**, 4702.
8 J. Wang, M. Xiao, W. Chen, M. Qiu, Z. Du, W. Zhu, S. Wen, N. Wang and R. Yang, *Macromolecules*, 2014, **47**, 7823.
9 L. Wang, S. Shi, D. Ma, S. Chen, C. Gao, M. Wang, K. Shi, Y. Li, X. Li and H. Wang, *Macromolecules*, 2015, **48**, 287.
10 Y. R. Cheon, Y. J. Kim, J. J. Ha, M. J. Kim, C. E. Park and Y. H. Kim, *Macromolecules*, 2014, **47**, 8570.
11 A. J. Heeger, *Adv. Mater.*, 2014, **26**, 10.
12 M. C. Scharber, D. Wuhlbacher, M. Koppe, P. Denk, C. Waldauf, A. J. Heeger and C. L. Brabec, *Adv. Mater.*, 2006, **18**, 789.
13 C. Cui, W. Y. Wong and Y. F. Li, *Energy Environ. Sci.*, 2014, **7**, 2276.
14 Y. Liang, Z. Xu, J. Xia, S. T. Tsai, Y. Wu, G. Li, C. Ray and L. Yu, *Adv. Energy Mater.*, 2010, **22**, E135.
15 F. Liu, Y. Gu, X. Shen, S. Ferdous, H. W. Wang and T. P. Russell, *Prog. Polym. Sci.*, 2013, **38**, 1990.
16 R. H. Lee and L. Y. Lee, *Colloid Polym. Sci.*, 2011, **289**, 1215.
17 G. Li, C. Kang, X. Gong, J. Zhang, C. Li, Y. Chen, H. Dong, W. Hu, F. Li and Z. Bo, *Macromolecules*, 2014, **47**, 4645.
18 C. Duan, K. S. Chen, F. Huang, H. L. Yip, S. Liu, J. Zhang, A. K. Y. Jen and Y. Cao, *Chem. Mater.*, 2010, **22**, 6444.
19 Y. Li, H. Xia, B. Xu, S. Wen and W. Tian, *J. Polym. Sci., Part A: Polym. Chem.*, 2008, **46**, 3970.
20 Y. T. Chang, S. L. Hsu, M. H. Su and K. H. Wei, *Adv. Mater.*, 2009, **21**, 2093.
21 Z. G. Zhang, S. Y. Zhang, J. Min, C. H. Chui, J. Zhang, M. J. Zhang and Y. F. Li, *Macromolecules*, 2012, **45**, 113.

22 J. H. Tsai, W. Y. Lee, W. C. Chen, C. Y. Yu, G. W. Hwang and C. Ting, *Chem. Mater.*, 2010, **22**, 3290.
23 Z. Gu, P. Shen, S. W. Tsang, Y. Tao, B. Zhao, P. Tang, Y. Nie, Y. Fang and S. Tan, *Chem. Commun.*, 2011, **47**, 9381.
24 H. J. Wang, L. H. Chan, C. P. Chen, S. L. Lin, R. H. Lee and R. J. Jeng, *Polymer*, 2011, **52**, 326.
25 N. Chakravarthi, K. Gunasekar, C. S. Kim, D. H. Kim, M. Song, Y. G. Park, J. Y. Lee, Y. Shin, I. N. Kang and S. H. Jin, *Macromolecules*, 2015, **48**, 2454.
26 S. Mei, F. Wu, Y. Huang, B. Zhao and S. Tan, *Eur. Polym. J.*, 2015, **67**, 31.
27 H. J. Wang, J. Y. Tzeng, C. W. Chou, C. Y. Huang, R. H. Lee and R. J. Jeng, *Polym. Chem.*, 2013, **4**, 506.
28 S. Li, J. Yuan, P. Deng, W. Ma and Q. Zhang, *Dyes Pigm.*, 2014, **106**, 121.
29 D. F. Zeigler, K. A. Mazzio and C. K. Luscombe, *Macromolecules*, 2014, **47**, 5019.
30 P. Zhou, D. Dang, J. Fan, W. Xiong, C. Yang, H. Tan, Y. Wang, Y. Liu and W. Zhu, *Dyes Pigm.*, 2015, **112**, 99.
31 Y. R. Liu, L. H. Chan and H. Y. Tang, *J. Polym. Sci., Polym. Chem. Ed.*, 2015, **53**, 2878.
32 K. Kranthiraja, K. Gunasekar, W. Cho, M. Song, Y. G. Park, J. Y. Lee, Y. Shin, I. N. Kang, A. Kim, H. Kim, B. Kim and S. H. Jin, *Macromolecules*, 2014, **47**, 7060.
33 D. Dang, P. Zhou, Q. Peng, K. He, H. Jiang, P. Yang, H. Tan, Y. Wang, Y. Liu, G. Lei and W. Zhu, *Dyes Pigm.*, 2014, **109**, 6.
34 H. Liang, X. Zhang, R. Peng, X. Ouyang, Z. Liu, S. Chen and Z. Ge, *Dyes Pigm.*, 2015, **112**, 145.
35 G. Zhang, Y. Fu, Z. Xie and Q. Zhang, *Sol. Energy Mater. Sol. Cells*, 2011, **95**, 1168.
36 S. Y. Shiau, C. H. Chang, W. J. Chen, H. J. Wang, R. J. Jeng and R. H. Lee, *Dyes Pigm.*, 2015, **115**, 35.
37 M. A. Naik, N. Venkatramaiah, C. Kanimozhi and S. Patil, *J. Phys. Chem. C*, 2012, **116**, 26128.
38 R. H. Lee and L. W. Liu, *Dyes Pigm.*, 2010, **84**, 190.
39 O. Kwon, S. Barlow, S. A. Odom, L. Beverina, N. J. Thompson, E. Zojer, J. L. Brédas and S. R. Marder, *J. Phys. Chem. A*, 2005, **109**, 9346.
40 C. Y. Huang, W. H. Lee and R. H. Lee, *RSC Adv.*, 2014, **4**, 48150.